Mid-IR (L-band) electro-optic photonics for nulling interferometry

Myriam Bonduelle[a], Guillermo Martin[a], Germain Garreau[b], Denis Defrère[b], Nadège Courjal[c], Roland Salut[c], and Laurent Robert[c]

[a]Univ. Grenoble Alpes, CNRS, IPAG, 38000 Grenoble, France
[b]Institute of Astronomy, KU Leuven, Celestijnenlaan 200D, 3001, Leuven, Belgium
[c]FEMTO-ST, Univ. Franche-Comté, 25030 Besançon, France

ABSTRACT

This work aims to present a complex mid-infrared (L-band : 3.4 µm - 4.1 µm) astrophotonic chip made in Lithium Niobate (LiNbO3), an electro-optic crystal, using Titanium diffused waveguides. The L-band presents several key characteristics interesting in astrophysics, notably for imaging and characterise young exo-planetary systems, as well as exo-zodiacal disks. With the increasing interest in exo-planetary science, new instruments and projects are focusing in the mid infrared, such as METIS (ground-based), NOTT (ground based), or LIFE (space-based). Combining such projects with photonics and on-chip beam combination will allow for more compact instruments, easing their integration on ground or, even more so, space based projects, hence the interest for improving the performances of photonic building blocks used for astrophysics.
Here, we are presenting building blocks such as Y-splitters, directional couplers, unbalanced beam splitters... that have been optimised for the L-band in Lithium Niobate. Although such blocks have already been developed in the mid-IR in this material, we are here using a different crystal orientation and newer design that are producing lower losses and birefringence. In particular, a 4-telescope mid-infrared combiner (linked to the NOTT project) was made in order to achieve nulling interferometry in the L-band. We show that we have relatively low loss waveguides, controlled photometric splitters (20/80 flux ratio), as well as functional couplers and beam splitting techniques. Furthermore, we will implement the electro-optic effect in this chip, in order to have internal modulation, and to be able to finely tune the fringes and improve the contrast, allowing for a step further into compact nulling interferometry.

Keywords: Astrophotonics, Nulling interferometry, L-band, Lithium Niobate, Integrated Optics, Y-splitters, Directional couplers, Titane Diffusion

1. INTRODUCTION

1.1 Context

The NOTT (Nulling Observations of Dust and Planets) instrument is an L'-band nulling interferometer, part of the Asgard consortium, an instrument suite in preparation for the VLTI visitor focus.[1] It aims at detecting young exoplanets near the snow line (hot Jupiters), as well as exo-zodiacal dust clouds. These science cases require high angular resolution and high contrast imaging, due to the flux ratio between these objects and their host star. For young planets, this flux ratio is minimal in the L-band (3.4 µm - 4.1 µm), up to 10^{-4},[2] as the planet is still emitting light from its formation process. NOTT aims at fulfilling these requirements through nulling (high contrast) interferometry (high angular resolution) in the L'-band (3.5 µm - 4.0 µm). Additionally, NOTT is an integrated nuller, meaning that the 4-telescope recombination is made through waveguides on a chip. The chip that will be used for the instrument is made of Gallium Lanthanum Sulfide (GLS), and the waveguides are created using Ultrafast Laser Inscription.[3] The on-sky demonstration of the NOTT instrument will pave the way for numerous applications of on-chip nulling interferometry in the mid-infrared, following already implemented bulk nullers such as BLINC,[4] KIN,[5,6] LBTI,[7,8] PFN,[9] or the integrated near-infrared nuller GLINT.[10,11] The

Corresponding author: Myriam Bonduelle
E-mail: myriam.bonduelle@univ-grenoble-alpes.fr

compactness of these instruments also allows to consider new applications, and in particular, space-based ones, such as the LIFE project.
In that context, we are presenting in this work a 4-telescope beam combiner for nulling interferometry, based on the design of the NOTT chips, but in a different material (Lithium Niobate, $LiNbO_3$), and with another fabrication method (Titane diffusion).

1.2 Nulling interferometry principle

The principle behind nulling interferometry is to cancel the light coming from a bright host object (star) so as to be able to see its fainter orbiting companions (exoplanet for instance). In a classical Bracewell configuration,[12] the light from the $\{star + object\}$ system is collected by two telescopes and recombined. Through a precise control of said recombination, a destructive interferometric fringe is generated at the angular position of the bright object, so as to cancel its light.
The interference pattern coming from the star $I_\star$ and the object I_o can be expressed as:

$$I_\star(\theta_\star) = 2I_\star(1 + cos(\frac{2\pi}{\lambda}B\theta_\star)) \tag{1}$$

$$I_o(\theta_o) = 2I_o(1 + cos(\frac{2\pi}{\lambda}B\theta_o)) \tag{2}$$

with $\theta_\star$ and θ_o the angles of the star and object respectively, and B the baseline (distance between the telescopes). Now considering that the star is on axis, we have $\theta_\star = 0$, that is to say a constructive fringe for the star in the centre of the interferogram. With the right baseline B, we can have $\frac{2\pi}{\lambda}B\theta_o = \pi$, resulting in a destructive fringe for the object. Finally, adding a π phase shift in one of the arms of the interferometer will inverse the system, resulting in a destructive fringe for the star and a constructive one for the planet.

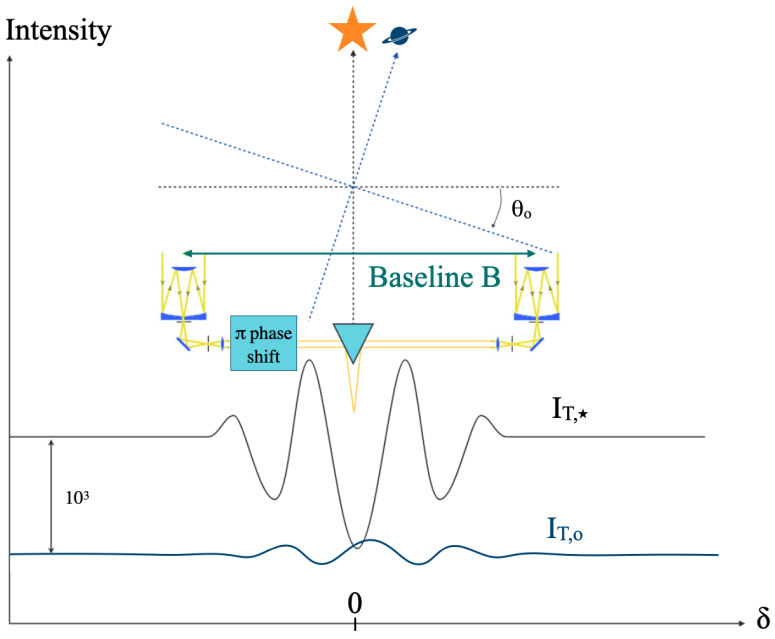

Figure 1: Principle of a Bracewell configuration to design an interferometric nuller. The star is observed on axis by two telescopes, and the off-axis object is at an angle θ_o from the star. With the right baseline and a π phase shift in one of the arms of the interferometer, the system is reversed, resulting in a constructive fringe for the object, and a destructive fringe for the star. These fringes are shown, in black for the star and blue for the object, with the x-axis represent the optical path difference δ and they-axis representing the intensity. Figure adapted from Heidmann.[13]

As can be seen in fig.1, the faint fringe pattern of the planet should be visible in the destructive fringe of the star. The performances of the interferometric nuller can be quantified by the null depth N, defined as:

$$N = \frac{1-C}{1+C} \tag{3}$$

With C the contrast, defined as:

$$C = \frac{I_{max} - I_{min}}{I_{max} + I_{min}} \tag{4}$$

In fig.1, the null depth obtained is 10^{-4}, allowing to faintly observe the signal from the planet in the nulled star fringe. In the case of the NOTT project, the required null depth at the output of the chip is 10^{-3} (allowing to obtain a contrast ratio sufficient for NOTT's science cases with additional post-processing).

2. NULLING CHIPS

2.1 Lithium Niobate

The material that was chosen to implement our photonic chip is Lithium Niobate ($LiNbO_3$), an electro-optic bi-refringent crystal, showing a Pockels effect. This non-linear effect allows to locally change the refractive index by applying an electric field. The variation of the refractive index Δn_{EO} as a function of the applied electric field is described by:

$$\Delta n_{EO} = -\frac{1}{2} \cdot n^3 \cdot r_{51} \cdot E_{app} \tag{5}$$

with n the refractive index of Lithium Niobate, r_{51} an electro-optic coefficient specific to lithium niobate (around 23 pm/V at 3.39 µm[14]), and E_{app} the applied electric field. This variation of the refractive index will, in turn, induce a phase shift $\Delta\Phi_{EO}$ of the fringes inside the material, through:

$$\Delta\Phi_{EO} = \frac{2\pi}{\lambda} \cdot \Delta n_{EO} L_{el} \tag{6}$$

with L_{el} the length of the electrodes.
Finally, E_{app} can also be expressed as a function of the voltage applied V and the gap between the electrodes w_{el}, through:

$$E_{app} = \frac{V}{w_{el}} \tag{7}$$

Combining eq.5, eq.6 and eq.7 allows to define the value V_π corresponds to the required voltage that needs to be applied to obtain a π phase shift of the fringes (i.e. $\Delta\Phi_{EO} = \pi$). This value can be determined theoretically using the different parameters of the problem, and was found to be around 60V for the V4 electrodes (L_{el} = 4.6mm and $w_{el} = 18$ µm). However, the experimental value can be quite different, due to the efficiency coefficient of the electrodes. This will be observed in section 4.2.
In this work, contrary to previous mid-IR combiners in Lithium Niobate,[13,15] our samples are made using z-cut Lithium Niobate (instead of x-cut). The choice of this cut allows have the Pockels effect impacting both the TE and TM polarisation with the same electro-optic coefficient, allowing to modulate both polarisations similarly.

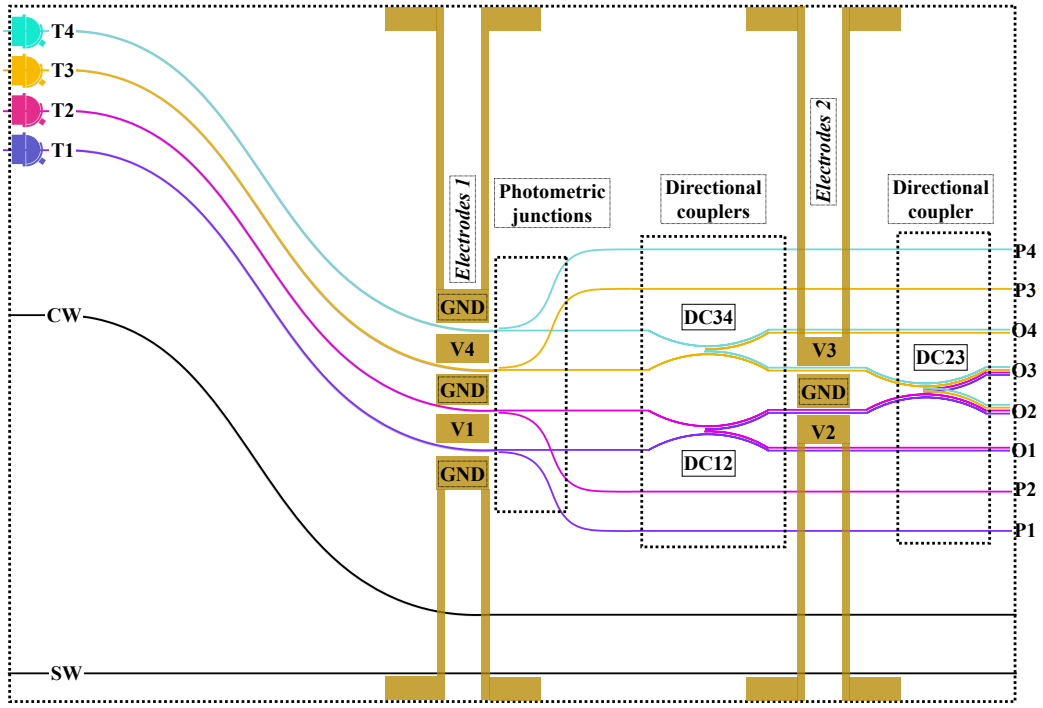

Figure 2: Design of the interferometric nulling chip. Each of the input channels (T1, T2, T3 and T4) are represented in a different colour, and the straight waveguide (SW) and reference curved waveguide (CW) are also shown in black. There is an initial S-bend to avoid stray light, then Y-junctions allowing to obtain the photometric outputs, and finally the three directional couplers (DC12, DC34 and DC23) allowing to obtain the interferences pattern. Finally, the electrodes used to implement the electro-optic effect are represented in golden-brown. Each of the interferometric outputs (O1, O2, O3 and O4) are showcased with the colours of the inputs that can be observed at this output.

2.2 Design

The interferometric chips that were implemented in the context of this project were designed following a double Bracewell configuration.[2] The design of the chip is presented in fig.2

The light from 4 telescopes (corresponding to the 4 VLTI telescopes) are injected onto 4 single mode waveguides. The first functions implemented is an S-bend in the waveguides, allowing to avoid stray light coming from the injection to pollute the outputs. Each of the inputs is then splitted through Y-junctions (directional couplers that allow for asymmetric flux distribution), so as to obtain P1, P2, P3 and P4, that will serve as the photometric references (extracting 20% of the flux). The main remaining channels (80% of the flux) are combined two-by-two through the DC12 and DC34 directional couplers: the flux interferes through evanescent coupling (50% / 50% flux distribution). Finally, the interferences resulting from those two-by-two combination are once again coupled through DC23, so as to obtain a double null configuration. In the specific case of the chip presented in this work, two sets of electrodes have been added so as to implement the electro-optic effect.

2.3 Fabrication method

All of the photonic functions implemented on the chip are Titanium Diffused waveguides in a z-cut $LiNbO_3$sample. They are made with a lithographic process: titanium ions are deposited in the material on chosen areas of the sample through the use of a mask. These ions then diffuse in Lithium Niobate, creating single-mode mid-infrared waveguides.[16] The obtained refractive index change Δn is at maximum around 10^{-2}, and this technique allows to guide both the TE and TM polarisations with similar -relatively low- propagation losses. The final step is

the implementation of the gold electrodes, deposited onto a thin substrate layer on top of the sample through a lithographic progress.

3. CHARACTERISTICS OF THE CHIP

Using the reference straight and curved waveguides (SW and CW), the propagation losses and bending losses of the chip were characterised:

- $\alpha_{prop} \sim 1.0$ dB/cm for the propagation losses
- $\alpha_{bending} \sim 0.3$ dB for the bending losses

The bending losses are relatively low, which is expected as the curvature radius that we implemented is long: $R_c \sim 341$ mm.
Each of the four inputs were then injected separately, using an HeNe 3.39µm laser. The obtained image on the detector (a FLIR camera) is shown in fig.3:

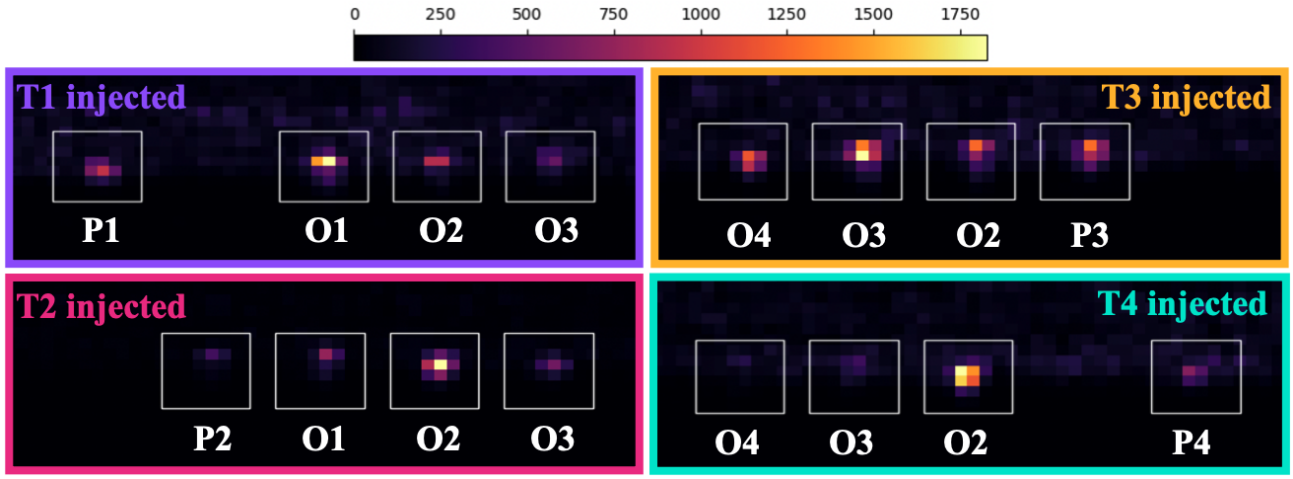

Figure 3: Outputs illuminated for each of the inputs injected (T1 in violet, T2 in pink, T3 in yellow, T4 in green). The results are as expected: one photometric output illuminated for each input, and three of the four interferometric outputs illuminated (O2 and O3 every time, and O1/O4 depending on the injected channel.

From these results, the splitting ratio for the directional couplers (both for the photometric outputs and the interferences) can be deduced. The photometric channels were expected to have 20% of the flux, and got on average 21.5%. The directional couplers used to create the interferences were supposed to split the flux in a 50/50 % ratio, and we obtain an average of 40/60%. Using the values of the propagation and bending losses previously calculated as references, the losses induced only by the photonic functions (one Y-junction for the photometric output and two successive directional couplers for each of the channel) can be obtained. For the best channel (the T3 injection), these losses have been found to be around 2.22 dB. The throughput of the chip can be deduced from this results, and is, for the complete chip, 4.3%. This is quite a low throughput, however the main losses are expected to come from propagation. The chip is currently 8.4cm long, meaning that reducing its length will allow to drastically improve the throughput.
These results are presented using unpolarised light, however the sample has also been injected using TE and TM polarised light. In the case of the reference waveguides SW and CW, both polarisation led to similar low propagation losses (as expected, see section 2.3). However, it is interesting to note that the remaining waveguides (T1, T2, T3 and T4 channels) are showing propagation losses much higher for TM light than for TE, due to the presence of electrodes around those channels. This was confirmed by tests on another sample, that contained only straight waveguides, some with electrodes and some without, and showed the same tendency: TM polarised light perfectly guided without any electrodes, and absorbed in the presence of the electrodes.

4. INTERFEROMETRIC RESPONSE

In order to study the interferometric response of the nulling chip, the T2 and T3 channels in fig.2 were injected simultaneously, through mirrors and a converging lens. The optical path was then modulated, either externally (section 4.1) or internally (section 4.2). The obtained interferogram can be described by the following equation:

$$I_T = I_1 + I_2 + 2 \cdot \sqrt{I_1 \cdot I_2} \cdot V \cdot cos(\frac{2\pi}{\lambda} \cdot \delta) \tag{8}$$

with I_1 and I_2 the flux from the two arms of the interferometer, V the visibility and δ the optical path difference (OPD). The OPD corresponds to the geometrical path difference multiplied by the refractive index in which this geometrical path difference happens. The visibility quantifies the maximum contrast that can be obtained, and depends on several parameters (the source, the instrument, the atmosphere...). In our case, the visibility is considered to depend only on the instrument itself (point-like source, and laboratory conditions). Finally, the corrected intensity, expressed as:

$$I_{corr} = 1 + \frac{I_{T,mes} - (I_1 + I_2)}{2 \cdot \sqrt{I_1 \cdot I_2}} \tag{9}$$

will be plotted.
With T2 and T3 injected, the P2, O1, O2, O3, O4, and P3 outputs are illuminated. O2 and O3 represent the interferometric outputs, where the light from T2 and T3 interfere through the DC23 coupler (whereas O1 and O4 are not interfering with any of the other channels), and P2 and P3 are the photometric outputs and will allow to obtain I_1 and I_2.

4.1 External modulation

The external modulation is implemented through one of the injection mirrors, that is mounted onto a motorised translation axis (Physik Instrumente). This allows to externally change the optical path difference (OPD), resulting in the modulation of the interferences in the O2 and O3 outputs. The corrected interferogram is presented in fig.4:

In fig.4, the O2 and O3 outputs are, as expected, in phase opposition, and the best contrast and null depth achieved can be obtained for both outputs (O2 and O3):

- best contrast for O2: 86%
- best null depth for O2: 7.10^{-2}
- best contrast for O3: 90%
- best null depth for O3: 5.10^{-2}

These results are very preliminary, and obtained on a bench not optimised for nulling interferometry. Several sources of errors can be identified, with, in particular, a strong effect of the photometric error: the flux injected in T2 and T3 inputs is not balanced. Unbalanced photometries will result in a loss of contrast, and a higher null depth.

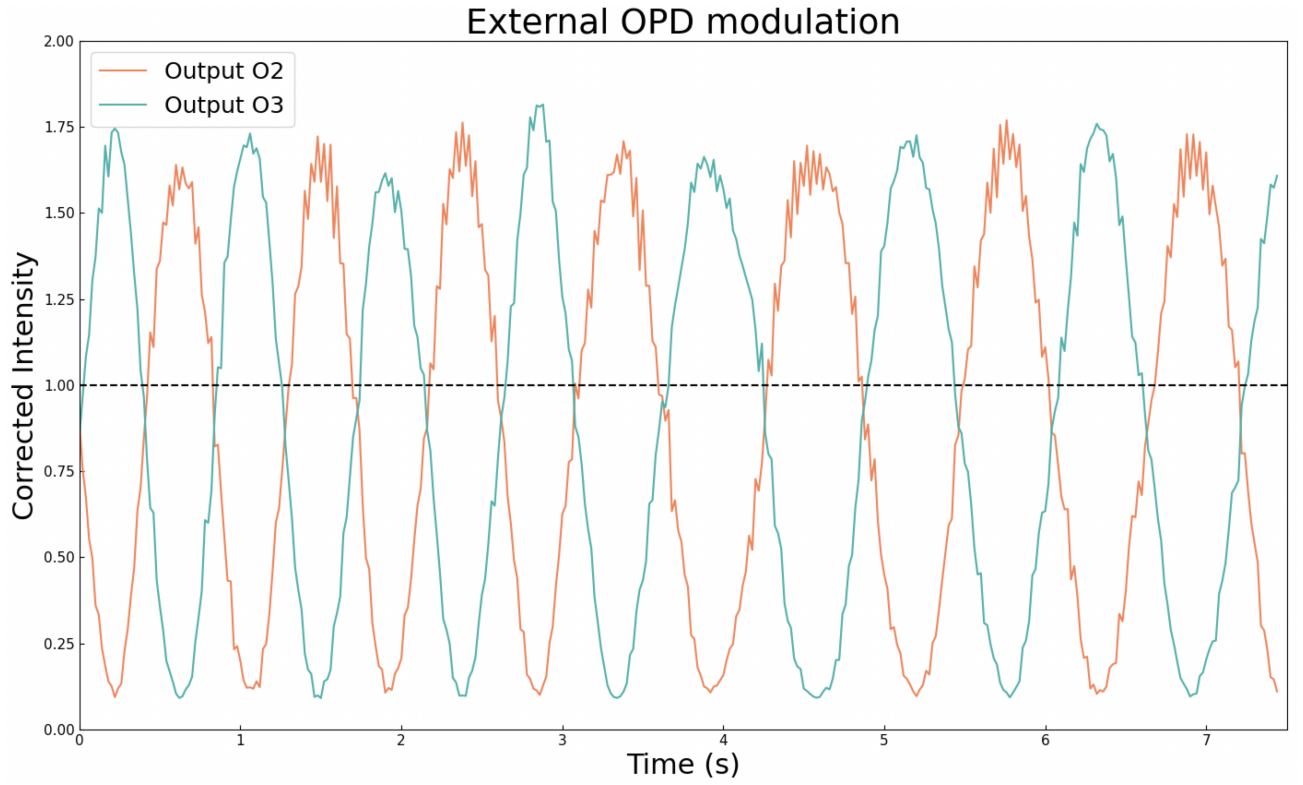

Figure 4: Outputs O2 (in coral) and O3 (blue-green) when T2 and T3 are injected. The optical path difference is externally modulated through a moving mirror, resulting in an interference pattern in phase opposition at the O2 and O3 outputs. The x-axis represents the time (in s) during which the OPD is modulated, and the y-axis the intensity at the two outputs, corrected following eq.9.

4.2 Internal modulation

The internal modulation is achieved through the electrodes, that allow to implement the electro-optic effect. In particular, the V4 electrode was connectorised, and a triangular electric ramp of 70 Volts from peak to peak was applied, allowing to locally modify the refractive index in the T3 waveguide. This, in turn, will change the optical path difference between T2 and T3, also resulting in the modulation of the interferences in the O2 and O3 outputs.

O2 and O3 remain in phase opposition, but the applied electric ramp is not enough to cover a full interferometric fringe. This results in a lower amplitude than previously, and the fact that each time the ramp reaches a peak (minima or maxima), the phase also changes its course. The value V_π, corresponding to the voltage required to obtain a π phase shift, i.e. $\Delta\Phi_{EO} = \pi$, can be deduced from fig.4 and fig.5. The values obtained are:

- $V_\pi^{exp} = 113$ V for the O2 output
- $V_\pi^{exp} = 122$ V for the O3 output

Theoretically, applying a ramp of around 120V should allow to obtain a π phase shift. To diminish the value V_π, and modulate several fringes, other parameters can be considered. In particular, the length of the electrodes L_{el} (see eq.6) and gap between the electrodes w_{el} (see eq.7) can be changed. In our case, V4 is 4.6mm long, which is relatively short. Implementing longer electrodes will allow to increase the efficiency of the electro-optic effect.

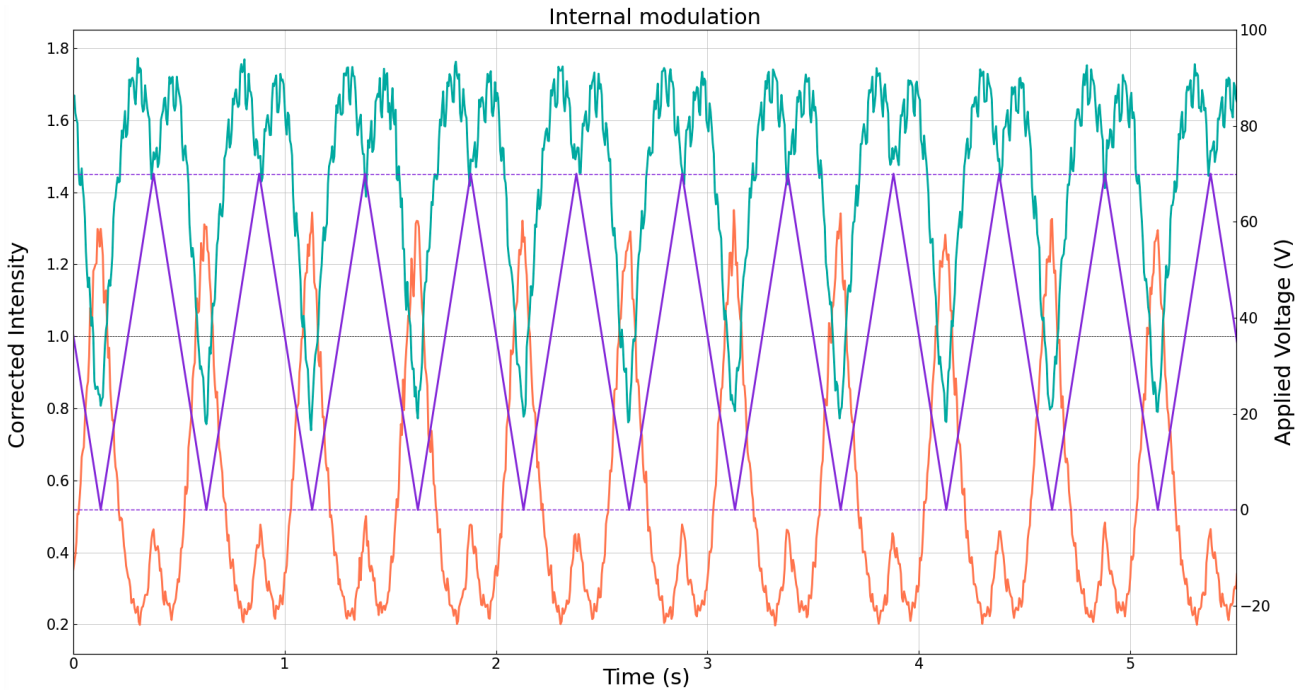

Figure 5: Outputs O2 (in coral) and O3 (blue-green) when T2 and T3 are injected. The optical path difference is internally modulated through the electro-optic effect, with a triangular electric ramp of 70 Volts (in violet) applied onto the V4 electrode. The x-axis represents the time (in s) during which the OPD is modulated, the y-axis (left) the intensity at the two outputs, corrected following eq.9, and the y-axis (right) the applied electric ramp.

5. CONCLUSION AND PERSPECTIVES

The chip that is presented in this work allowed to obtain very promising results: the directional couplers (for both the photometric and interferometric outputs) behaved as expected, splitting the flux with ratios very close to what was expected, and the electro-optic effect was successfully implemented. As this chip is a first test-run, this is very promising for future technological iterations. In newer design, to gain in throughput, the length of the chip could be reduced by removing the initial S-bend (a gain of a few cm), or increasing the curvature radius of the initial S-bend -although at the cost of higher bending losses. As the absorption of the TM polarisation results from the deposition process of the electrodes, another method could also be studied, so as to ensure that both polarisations are correctly guided. Finally, designs for achromatic couplers could be envisioned, with, for instance, the use of the electro-optic effect,[17] asymmetric directional couplers,[18] multimode interference couplers,[19] or, more recently, tricouplers.[20]
Additionally, still using the current chip, a null closer to the required value (10^{-3}) could be obtained with tailoring the bench for nulling interferometry (balancing the photometries, allow for a 4-telescope injection instead of 2-T one...) which should allow to deepen the obtained null, and represents our short-term focus.

ACKNOWLEDGMENTS

IPAG Funding: Authors acknowledge the funding from Labex FOCUS (ANR-11-LABX-0013) and ASHRA (Action Specifique Haute Resolution Angulaire) from INSU-CNRS.
FEMTO-ST Funding: These works have been partially done within the French RENATECH network through its FEMTO-ST technological facility
KU-Leuven Funding: SCIFY has received funding from the European Research Council (ERC) under the European Union's Horizon 2020 research and innovation program (grant agreement CoG - 866070). This project

has received funding from the European Union's Horizon 2020 research and innovation programme under grant agreement No 101004719.

REFERENCES

[1] Martinod, M.-A., Defrère, D., Ireland, M., Kraus, S., Martinache, F., Tuthill, P., Bigioli, A., Bryant, J., Chhabra, S., Courtney-Barrer, B., Crous, F., Cvetojevic, N., Dandumont, C., Garreau, G., Lagadec, T., Laugier, R., Mortimer, D., Norris, B., Robertson, G., and Taras, A., "High-angular resolution and high-contrast vlti observations from y to l band with the asgard instrumental suite," (2023).

[2] Defrère, D., Bigioli, A., Dandumont, C., Garreau, G., Laugier, R., Martinod, M.-A., Absil, O., Berger, J.-P., Bouzerand, E., Courtney-Barrer, B., Emsenhuber, A., Ertel, S., Gagne, J., Glauser, A. M., Gross, S., Ireland, M. J., Kenchington, H.-D., Kluska, J., Kraus, S., Labadie, L., Laborde, V., Leger, A., Leisenring, J., Loicq, J., Martin, G., Morren, J., Matter, A., Mazzoli, A., Missiaen, K., Salman, M., Ollivier, M., Raskin, G., Rousseau, H., Sanny, A., Verlinden, S., Vandenbussche, B., and Woillez, J., "L-band nulling interferometry at the vlti with asgard/hi-5: status and plans," (2022).

[3] Sanny, A., Gross, S., Labadie, L., Defrère, D., Bigioli, A., Laugier, R., Dandumont, C., and Withford, M., "Development of the four-telescope photonic nuller of Hi-5 for the characterization of exoplanets in the mid-IR," in [*Optical and Infrared Interferometry and Imaging VIII*], Mérand, A., Sallum, S., and Sanchez-Bermudez, J., eds., *Society of Photo-Optical Instrumentation Engineers (SPIE) Conference Series* **12183**, 1218316 (Aug. 2022).

[4] Hinz, P. M., Angel, J. R. P., Hoffmann, W. F., McCarthy, D. W., McGuire, P. C., Cheselka, M., Hora, J. L., and Woolf, N. J., "Imaging circumstellar environments with a nulling interferometer," **395**, 251–253 (Sept. 1998).

[5] Colavita, M. M., Serabyn, E., Millan-Gabet, R., Koresko, C. D., Akeson, R. L., Booth, A. J., Mennesson, B. P., Ragland, S. D., Appleby, E. C., Berkey, B. C., Cooper, A., Crawford, S. L., Creech-Eakman, M. J., Dahl, W., Felizardo, C., Garcia-Gathright, J. I., Gathright, J. T., Herstein, J. S., Hovland, E. E., Hrynevych, M. A., Ligon, E. R., Medeiros, D. W., Moore, J. D., Morrison, D., Paine, C. G., Palmer, D. L., Panteleeva, T., Smith, B., Swain, M. R., Smythe, R. F., Summers, K. R., Tsubota, K., Tyau, C., Vasisht, G., Wetherell, E., Wizinowich, P. L., and Woillez, J. M., "Keck interferometer nuller data reduction and on-sky performance," *Publications of the Astronomical Society of the Pacific* **121**(884), 1120–1138 (2009).

[6] Serabyn, E., Mennesson, B., Colavita, M. M., Koresko, C., and Kuchner, M. J., "The keck interferometer nuller," *The Astrophysical Journal* **748**, 55 (mar 2012).

[7] Hinz, P. M., Defrère, D., Skemer, A., Bailey, V., Stone, J., Spalding, E., Vaz, A., Pinna, E., Puglisi, A., Esposito, S., Montoya, M., Downey, E., Leisenring, J., Durney, O., Hoffmann, W., Hill, J., Millan-Gabet, R., Mennesson, B., Danchi, W., Morzinski, K., Grenz, P., Skrutskie, M., and Ertel, S., "Overview of LBTI: a multipurpose facility for high spatial resolution observations," in [*Optical and Infrared Interferometry and Imaging V*], Malbet, F., Creech-Eakman, M. J., and Tuthill, P. G., eds., *Society of Photo-Optical Instrumentation Engineers (SPIE) Conference Series* **9907**, 990704 (Aug. 2016).

[8] Ertel, S., Defrère, D., Hinz, P., Mennesson, B., Kennedy, G. M., Danchi, W. C., Gelino, C., Hill, J. M., Hoffmann, W. F., Mazoyer, J., Rieke, G., Shannon, A., Stapelfeldt, K., Spalding, E., Stone, J. M., Vaz, A., Weinberger, A. J., Willems, P., Absil, O., Arbo, P., Bailey, V. P., Beichman, C., Bryden, G., Downey, E. C., Durney, O., Esposito, S., Gaspar, A., Grenz, P., Haniff, C. A., Leisenring, J. M., Marion, L., McMahon, T. J., Millan-Gabet, R., Montoya, M., Morzinski, K. M., Perera, S., Pinna, E., Pott, J. U., Power, J., Puglisi, A., Roberge, A., Serabyn, E., Skemer, A. J., Su, K. Y. L., Vaitheeswaran, V., and Wyatt, M. C., "The HOSTS Survey for Exozodiacal Dust: Observational Results from the Complete Survey," *Astronomical Journal* **159**, 177 (Apr. 2020).

[9] Mennesson, B., Hanot, C., Serabyn, E., Liewer, K., Martin, S. R., and Mawet, D., "High-contrast Stellar Observations within the Diffraction Limit at the Palomar Hale Telescope," **743**, 178 (Dec. 2011).

[10] Norris, B. R. M., Cvetojevic, N., Lagadec, T., Jovanovic, N., Gross, S., Arriola, A., Gretzinger, T., Martinod, M.-A., Guyon, O., Lozi, J., Withford, M. J., Lawrence, J. S., and Tuthill, P., "First on-sky demonstration of an integrated-photonic nulling interferometer: the GLINT instrument," *Monthly Notices of the Royal Astronomical Society* **491**, 4180–4193 (11 2019).

[11] Lagadec, T., Norris, B., Gross, S., Arriola, A., Gretzinger, T., Cvetojevic, N., Martinod, M. A., Jovanovic, N., Withford, M., and Tuthill, P., "The GLINT South testbed for nulling interferometry with photonics: Design and on-sky results at the Anglo-Australian Telescope," *Publications of the Astronomical Society of Australia* **38**, e036 (Aug. 2021).

[12] Bracewell, R. N., "Detecting nonsolar planets by spinning infrared interferometer," *Nature* **274**, 780–781 (Aug. 1978).

[13] Heidmann, S., *Composants actifs en optique intégrée pour l'interférométrie stellaire dans le moyen infrarouge*, PhD thesis (2013). Thèse de doctorat dirigée par Benech, Pierre et Martin, Guillermo Optique et radiofréquence Grenoble 2013.

[14] Nikogosyan, D., [*Nonlinear Optical Crystals: A Complete Survey*], Springer Science+Business Media, Inc., 2005 (2005).

[15] kai Hsiao, H., Winick, K. A., Monnier, J. D., and Berger, J.-P., "An infrared integrated optic astronomical beam combiner for stellar interferometry at 3-4 μm," *Opt. Express* **17**, 18489–18500 (Oct 2009).

[16] Courjal, N., Bernal, M.-P., Caspar, A., Ulliac, G., Bassignot, F., Gauthier-Manuel, L., and Suarez, M., [*Lithium Niobate Optical Waveguides and Microwaveguides*], IntechOpen, Rijeka (2018).

[17] Martin, G., Heidmann, S., Rauch, J.-Y., Jocou, L., and Courjal, N., "Electro-optic fringe locking and photometric tuning using a two-stage mach–zehnder lithium niobate waveguide for high-contrast mid- infrared interferometry," *Proc SPIE, Optical Ingineering* **53** (03 2014).

[18] Takagi, A., Jinguji, K., and Kawachi, M., "Wavelength characteristics of (2 2) optical channel-type directional couplers with symmetric or nonsymmetric coupling structures," *Journal of Lightwave Technology* **10**, 735–746 (June 1992).

[19] Kenchington Goldsmith, H.-D., Ireland, M., Ma, P., Cvetojevic, N., and Madden, S., "Improving the extinction bandwidth of mmi chalcogenide photonic chip based mir nulling interferometers," *Optics Express* **25**, 16813 (07 2017).

[20] Klinner-Teo, T., Martinod, M.-A., Tuthill, P., Gross, S., Norris, B., and Leon-Saval, S., "Achromatic design of a photonic tricoupler and phase shifter for broadband nulling interferometry," *Journal of Astronomical Telescopes, Instruments, and Systems* **8**, 045001 (Oct. 2022).